Volume 1 | Number 1 | Jan 2013 | Pages 1–100

Journal of
Materials Chemistry A

Materials for energy and sustainability
www.rsc.org/materialsA

ROYAL SOCIETY
OF CHEMISTRY

ROYAL SOCIETY
OF CHEMISTRY

www.rsc.org/materialsA

Colloidal Sb$_2$S$_3$ Nanocrystals: Synthesis, Characterization and Fabrication of Solid-State Semiconductor Sensitized Solar Cell

Mutalifu Abulikemu[1], Silvano Del Gobbo[1], Dalaver H. Anjum[2], Mohammad Azad Malik[3*], Osman M. Bakr[1*]

[1] Division of Physical Sciences and Engineering, Solar and Photovoltaic Engineering Research Center (SPERC), King Abdullah University of Science and Technology (KAUST), 23955-6900 Thuwal, Saudi Arabia.

[2] Imaging and Characterization Lab, King Abdullah University of Science and Technology (KAUST), 4700 KAUST, Thuwal, 23955-6900 Saudi Arabia

[3] School of Materials, The University of Manchester, Oxford Road, Manchester M13 9PL, UK

*Corresponding author. E-mail: osman.bakr@kaust.edu.sa; azad.malik@manchester.ac.uk

Abstract

Inorganic nanocrystals composed of earth-abundant and non-toxic elements are crucial to fabricated sustainable photovoltaic devices in large scale. In this study, various-shaped and different phases of antimony sulfide nanocrystals, which is composed of non-scarce and non-toxic elements, are synthesized using hot-injection colloidal method. The effect of various synthetic parameters on the final morphology is explored. Also, foreign ion (Chlorine) effects on the morphology of Sb$_2$S$_3$ nanocrystals have been observed. Structural, optical and morphological properties of the nanocrystals were investigated, and Sb$_2$S$_3$ nanocrystal-based solid-state semiconductor-sensitized solar cells were fabricated using as-prepared nanocrystals. We achieved promising power conversion efficiencies of 1.48%.

Binary chalcogenide semiconductors[1-9] have exhibited great potential for solar energy conversion due to their solution processability, bandgap tunability, large light absorption coefficient, and compositional tailorability. All high-performing photovoltaic materials contain either toxic or scarce elements, such as Pb, Cd, In, Ga and Te; thus, the production of solution-processable nanocrystals from earth-abundant and non-toxic elements using environmentally benign synthetic methods has become a major challenge for the inorganic semiconductor-based solar energy field. Antimony sulfide[3, 10-18] is one of the potential materials for use in low-cost solar cells because of its relatively high abundance, low toxicity and large light absorption coefficient.

Sb_2S_3[19-22] is known to exist in two distinct phases, amorphous and crystalline; Amorphous Sb_2S_3 is a direct bandgap semiconductor with a gap of 2.15 eV having a bright orange color. Crystalline Sb_2S_3 known as stibnite (gray black) has a bandgap of 1.73 eV and was demonstrated to be suitable for potential applications in solar cells,[3, 10-18] optical data storage,[21] lithium batteries [23] and supercapacitors.[24] Sb_2S_3 has already been used in high-performance semiconductor-sensitized solar cells[3] as a light harvester due to its high absorption coefficient.[25] Sb_2S_3 can form stable complexes with bifunctional hole-transporting materials in semiconductor sensitized solar cells (SSSCs),[10] a key feature for high-efficiency semiconductor-sensitized inorganic-organic hetero-junction solar cells. Early work on Sb_2S_3-based solar cells dates to 1992, when Savadogo *et al.* made photoelectrochemical cells with 0.8% and 2.0% efficiencies under 40 mW/cm^2 illumination for amorphous and crystalline Sb_2S_3, respectively.[26] Recently, a 7.5% efficiency was obtained[3], where the Sb_2S_3 is deposited on TiO_2 using a chemical bath deposition (CBD) method. More recently, 0.98% device efficiency was achieved using single molecule precursor antimony ethyl xanthate[17]. However, to the best our knowledge, there are no reports on Sb_2S_3 NCs-based solar cells. Besides Sb_2S_3, the narrower band gap Sb_2Se_3 was also utilized as light absorbed for thin film solar cells obtaining remarkable values of efficiency.[8, 9]

Various shapes of Sb_2S_3 NCs have been synthesized using hydrothermal,[22, 24, 27-29] solvothermal,[13, 28, 30] polyol,[31] chemical vapor transport reactions,[28]Aerosol-Assisted Chemical Vapour Deposition

(AACVD)[32-34] and chemical bath deposition.[21] Oxygen contamination was a problem in most of the cases. A report on the synthesis of Sb_2S_3 nanowires using the hot injection method is already present in literature,[12] but no systematic studies of the synthesis of amorphous (orange) and crystalline (gray-black) Sb_2S_3 NCs using colloidal hot injection methods have ever been reported. Herein we report a systematic study on hot-injection colloidal synthesis of Sb_2S_3 NCs and an investigation into the effect of precursors, temperature and time on the formation of Sb_2S_3 NCs. We also report the fabrication of Sb_2S_3 NCs-based solar cells and the characterization of their photovoltaic performance.

The synthesis of Sb_2S_3 NCs was carried out under inert conditions. In a typical synthesis of Sb_2S_3 NCs (please refers to the detailed experimental section in the SI), 1 mmol of antimony (III) chloride, 6 ml oleic acid and 8 ml 1-octadecene (ODE) were loaded into a 3-neck round-bottom flask and heated (150°C) under vacuum for 1h, and then purged and kept under nitrogen while maintaining the temperature at 180 °C. A total of 1.5 mmol *bis*(trimethylsilyl) sulfide (TMS) in 5 ml ODE was then injected into the reaction flask which changed the color of the solution from clear yellow to orange. The reaction temperature was gradually decreased to 100 °C after injection. After approximately 30 minutes, the orange color of the solution started to change into a grey-black color, and the reaction was stopped after 90 minutes. In order to observe the growth of NCs soon after the injection, a 5 ml aliquot was collected after 90 s of injection, and quenched by injecting it into cold anhydrous toluene. Then, the final product and the aliquot in toluene were washed by centrifugation with a mixture of chloroform and ethanol, and eventually re-dispersed in toluene.

The aliquot taken after 90 s of the injection was an orange solution which was analyzed by powder X-Ray diffraction (p-XRD). The broad p-XRD pattern corresponds to the stibnite (Sb_2S_3; ICDD # 00-006-0474) phase of antimony sulfide (Figure 1a). The broadness of the pattern indicates a poorly crystalline Sb_2S_3 sample. The color of the reaction mixture turned gray-black after the completion of the reaction, and the p-XRD pattern in Figure 1b shows that the as-prepared NCs are highly crystalline and with no indication of secondary phases.

In order to characterize the optical properties of the as-synthesized orange and gray-black Sb_2S_3 NCs and to determine their band gap, a NCs film was deposited on a clean glass substrate. Figure 2 shows the Tauc plot of crystalline gray-black and orange semi-amorphous Sb_2S_3 NPs deposited on glass substrates. From the onset of the curves it was possible to estimate the bandgaps of the two films to be 1.73 eV for gray-black Sb_2S_3 NCs – close to the band gap of bulk crystalline Sb_2S_3 [22] and 2.15 eV for the orange Sb_2S_3 NCs. Transmission electron microscopy (TEM) analysis of the samples is carried out in Titan G2 80-300CT instrument from FEI Company which was also attached with an X-ray energy dispersive spectroscopy (EDS) capability. Conventional TEM, high-resolution TEM (HRTEM), and selected area electron diffraction (SAED) measurements were carried out to determine the shape, size, and crystallinity of as-synthesized NCs. TEM micrographs (Figure 3a and b) show that the particles constituting the orange powder obtained from the 90 s aliquot, have a spherical shape and are connected in a chain-like structure. The average size of the NCs is approximately 30 nm. The SAED pattern (Figure 3b) indicates that the NCs are weakly crystalline since the Debye-Sherrer rings are rather fuzzy. Based on the color of the NCs and the results from both p-XRD and SAED techniques, the as-synthesized NCs are poorly crystalline Sb_2S_3 NCs. EDX analysis was carried out to determine the stoichiometry of NCs by measuring the atomic percentage ratio of Sb to S. The ratio was found to be 42:58, as shown in Figure S1, indicating that the Sb_2S_3 NCs are slightly antimony rich.

Other TEM micrographs (Figures 3c and d) show that the NCs obtained after the completion of the reaction have an urchin-like nanostructure composed of nanorods (NRs). HRTEM micrographs (Figure 3d) indicate that the Sb_2S_3 NCs are highly crystalline, with a diameter of approximately 15 nm. The high crystallinity of these NCs is further affirmed by SAED (Figure 3d). The corresponding EDX spectrum (Figure S2) of crystalline NCs confirmed that the crystalline phase is also stoichiometric, with an atomic ratio of Sb to S of 40:60. These results show that the shape, size and stoichiometry of Sb_2S_3 NCs can be controlled by the reaction time.

Other sulfur sources were used instead of TMS to observe their effect on the morphology of Sb_2S_3. In one case elemental sulfur was dissolved in degassed oleylamine (1 mmol elemental S in 3 ml oleylamine) and stored in a glove box as a stock solution. A total of 1.5 mmol sulfur stock solution was injected instead of the TMS solution, and all other conditions remained unchanged. Similar to the previous experiment, one aliquot was taken at 90 s, and the same cleaning process was used. The corresponding TEM micrographs of NCs synthesized for 90 s are shown in Figures S3a and b, are of spherical shape and are connected in a chain-like structure. Their average size is approximately 20 nm, smaller than NCs synthesized using TMS solution in figure 3b. The color of the as-synthesized NCs is orange suggesting they are weakly crystalline. After approximately 40 minutes, the orange color of the solution in the flask started turning to black. The reaction was stopped after 90 minutes following the injection. Figures S3c and d show that the morphology is that of highly crystalline nanorods. However, evidence from TEM and EDS (Figure S4) indicates that some antimony NCs formed on the surface of the Sb_2S_3 NCs, suggesting that part of the $SbCl_3$ was reduced to Sb by the oleylamine. Another experiment with a second injection of the sulfur source was performed to obtain pure Sb_2S_3 nanorods (NRs) free from Sb NPs. During the experiment, a 0.75 mmol sulfur stock solution was injected once the orange color of solution started changing into black after the initial injection of the 1.5 mmol sulfur stock solution. TEM images (Figures S3e and f) indicate that there are no Sb NCs on the surface of the NRs. The reactivity of the elemental S in oleylamine is lower than in TMS, which may lead to a slower and anisotropic growth of Sb_2S_3 NCs.

As another sulfur source, it was used elemental S in ODE. This sulfur solution shows has the advantage to be stable in air [35]. The stock solution was prepared by dissolving 1 mmol S in 6 ml ODE under nitrogen at 200°C for 1 h. Two rounds of experiments were carried out: one in which the reaction temperature was decreased to 100°C after the injection of the 1.5 mmol sulfur source and another in which the reaction temperature was maintained at 180°C following the injection. In both cases, there was no formation of NCs. Another experiment was carried out at 220°C, with the solution maintained for 90 minutes at that temperature. We only obtained black NCs, and could not obtain orange NCs by this method. This outcome may be due to the lower reactivity of elemental sulfur in ODE that requires higher temperatures.

Similar observation was reported by Guo *et al*.[36] for the formation of CdS NCs when diphenyl disulfide

was used as a sulfur source. The TEM analysis combined with EDS measurements shown in Figure S4

indicate that the as-synthesized NCs is composed of crystalline Sb_2S_3 with a nanorod-like morphology.

Even in this case Sb NCs were observed on the surface of the Sb_2S_3 NCs.

The injection and NC growth temperature can affect the size, shape, monodispersity, and phase of NCs.[37]

Several experiments were carried out to explore the effect of temperature on the size and morphology of

Sb_2S_3 NCs as well as on the reaction kinetics of the formation of Sb_2S_3 NCs. TMS solution was injected

at 140°C, and all other conditions were the same. An orange aliquot was taken 90s after the injection, and

a second one was taken after 90 minutes, resulting in a mixture of orange and black colors. We took a

third aliquot after 2 h, which had a completely black color. The TEM micrograph (Figure S5a) of the first

aliquot indicates that it is composed of spherical amorphous Sb_2S_3 NCs, and TEM and HRTEM images

(Figures S5b and c) of the second aliquot show that the as-synthesized NCs are a mixture of amorphous

and crystalline Sb_2S_3. TEM, HRTEM and SAED (Figures S5d-f) confirmed that the third aliquot was

made up of pure crystalline Sb_2S_3 NCs. The diameter of the NRs was smaller than that of the crystalline

Sb_2S_3 NCs obtained when the injection temperature was 180 °C. Thus, the lower injection temperature

affected, as expected the diameter of the NRs and the kinetics of formation of the crystalline Sb_2S_3 NCs.

To further quantify the effect of a high injection temperature, TMS solution was injected at 220 °C. The

TEM and SAED micrographs (Figure S6) of an aliquot of as-synthesized NCs, taken 90s after the

injection, indicate that the NCs consist of amorphous and crystalline Sb_2S_3. After the TMS injection, the

solution color immediately changed to orange and subsequently started turning black. The shape of the

crystalline Sb_2S_3 NCs was irregular, resembling a nanobelt structure. This finding further demonstrates

how injection temperature affects the morphology and kinetics of formation of Sb_2S_3 NCs.

In another trial, TMS solution was injected at 100 °C, and this temperature was maintained throughout the

reaction. It took more than 2.5 h to form completely black NCs. Thus, it takes a longer time to form

crystalline Sb_2S_3 NCs if the TMS solution is injected at a lower temperature. However, the diameter of the crystalline NCs (Figure 5b) is larger than for the NCs obtained with injection at 140 °C or 180 °C.

We also designed another experiment to grow Sb_2S_3 NCs at a higher growth temperature. In this experiment, TMS solution was injected at 140 °C, and the reaction temperature was maintained at 140°C. Highly crystalline Sb_2S_3 NCs were obtained, as shown in Figures S7 a-c. Compared to NCs grown at the lower temperature (100 °C, Figure S7 d-f), the diameter of the NRs was larger.

Based on these experiments that were carried out at different nucleation (injection) and growth temperatures (Figure 4, S5-7), it can be concluded that lower nucleation (injection) temperatures lead to lower monomer concentrations that can yield larger-sized nuclei. On the other hand, larger particles can be obtained by higher growth temperatures as the rate of the monomer addition to existing particles is increased. Moreover, there is a higher chance of Ostwald ripening at higher temperatures.[37] Very high temperatures (T>180 °C), cause an even higher monomer concentration as well as a faster kinetics that give rise to larger NPs in a shorter time lapse.

Sb_2S_3 NCs were also synthesized using antimony (III) acetate and oxide as Sb precursors. The corresponding TEM and SAED micrographs are shown in Figure 6a and b. The color of both solutions was orange, indicating that they were both composed of weakly crystalline Sb_2S_3 NCs. The as-synthesized NCs were well separated with a spherical shape and an average size of approximately 125 nm. The size of the NCs did not change significantly after 90 minutes of reaction time. Similarly, Sb_2S_3 NCs were synthesized using Sb_2O_3 instead of $Sb(OAc)_3$, and the TEM micrographs (Figure 6 c and d) show that the as-synthesized NCs are spherical in shape, with an average size of approximately 100 nm, smaller than for NCs synthesized using $Sb(OAc)_3$. SAED (Figure 6d insert) confirmed that the NCs synthesized for 90 minutes were weakly crystalline. In both cases, the experiments were continued overnight, but the orange color did not change. It is thus straightforward that the counter ion of the precursor plays an important role on the morphology and crystallinity; in fact it is known that crystalline chain-like NRs are formed when $SbCl_3$ is used as an antimony precursor.[38]

To see the effect of a higher temperature on the morphology of NCs, the temperature was maintained at 180 °C. After 1.5 h of reaction time, the orange color of the NCs started changing to black, and the reaction was stopped after 2 h. TEM, HRTEM and SAED micrographs (Figure S8) indicate that the as-prepared NCs were highly crystalline and composed of large NRs with a diameter larger than 200 nm.

Foreign ion effects on the morphology of metal and semiconductors NCs have been also observed.[39-41] As can be noted above we could not obtain highly crystalline black Sb_2S_3 NCs when antimony acetate or oxide were used as an antimony source under the same reaction conditions. We suspected that this effect may be due to the role of chlorine ions.[40]. To study this effect, different amounts of 3 and 6 mmol NaCl in 0.5 ml H_2O were added to the mixture of $Sb(OAC)_3$, oleic acid and ODE, with the other conditions and details of the procedure the same as before. The reaction was carried out at different time lengths, but all of the as-synthesized NCs were orange Sb_2S_3 NCs. TEM and SAED micrographs (Figures S9) indicate that there is weak crystallinity in the product, with some spherical NCs of both large and small sizes. The reason that NaCl did not induce a morphology change is that chlorine ions may not participate in the metal-organic complex in this reaction due to water's miscibility with oleic acid and ODE.

For a follow-up trial, tetrabutylammonium chloride (NBu_4Cl) was chosen as a chlorine source soluble in ODE, and 3 mmol NBu_4CI were added to the mixture of $Sb(OAC)_3$, oleic acid and ODE. The orange color started to change to black half an hour after the TMS injection, and the second aliquot was taken after 90 minutes of reaction time. TEM, HRTEM and SAED micrographs (Figures 6) reveal that weakly crystalline and crystalline Sb_2S_3 NCs were obtained. The shape of the amorphous NCs is chain-like spherical, whereas the shape of the crystalline NCs is chain-like NRs with a diameter of approximately 20 nm. We were therefore able to control the morphology of Sb_2S_3 NCs by adding a proper chlorine source, *i.e.*, NBu_4Cl. It is necessary to remark that NBu_4Cl has a good solubility in the mixture of oleic acid and ODE at an elevated temperature.

The photovoltaic properties of Sb_2S_3 NCs were investigated by fabricating a device with the quite common solid state sensitized solar cell (SSSC) architecture HTM/Absorber/ETM/FTO. Orange Sb_2S_3

NCs are used as starting materials for Sb_2S_3-based SSSCs because of their higher dispersability, and then annealed at 300 °C for 30 minutes to form crystalline Sb_2S_3 NPs film. In a typical device fabrication process, Sb_2S_3 NCs were deposited on mesoporous TiO_2-coated FTO using the dip coating technique, and then annealed under inert conditions. After that, a 2,2',7,7'-Tetrakis(N,N-di-p-methoxyphenylamino)-9,9'-spirobifluorene (spiro-OMeTAD) solution was spin-coated as a HTM, and gold was thermally evaporated as a top electrode.   The detailed device fabrication process was described in supporting information (SI). Optical absorption measurements on the annealed films demonstrate that the band gap of Sb_2S_3 is nearly identical to the crystalline gray-black Sb_2S_3 NCs (Figure S10), and SEM images indicated that the individual NCs were merged to form larger structures after annealing (Figure S11). In order to improve surface passivation of absorber layer for reducing charge recombination at interface, a thin layer of ZnS is coated on the surface of Sb_2S_3 NCs film. PL spectra (Figure S12) showed that the PL intensity is significantly enhanced after the ZnS surface treatment indicating that the surface defects are decreased by passivation. From the J-V curve under illumination of the as-fabricated device (Figure 4 7) a 1.48% power conversion efficiency was obtained, with short circuit current J_{sc}=7.15 mA/cm^2, open circuit voltage V_{0C}=421 mV and fill factor FF=49.27 %. The average cell efficiency coated with ZnS is higher than the cell without ZnS-coating of 36%. The band gap of Sb_2S_3 can be lowered by doping with selenium to boost the short-circuit current density.[8, 9, 42].

In conclusion, a synthesis protocol was established for novel, nanostructured, Sb_2S_3 NC photovoltaic materials, and their structural, morphological, optical, and photovoltaic properties were characterized. The main achievement of this work is the development of a colloidal, hot-injection synthetic protocol that enables the production of various shapes of Sb_2S_3 NCs for inks for use in the fabrication of low-cost, environmentally friendly PV cells. Moreover, different antimony and sulfur sources and the effects of foreign ions on the shape and crystallinity of Sb_2S_3 NCs were also examined. Finally, for the first time, Sb_2S_3 NC-based SSSCs were fabricated via dip coating, exhibiting promising power conversion efficiencies to warrant further investigation.
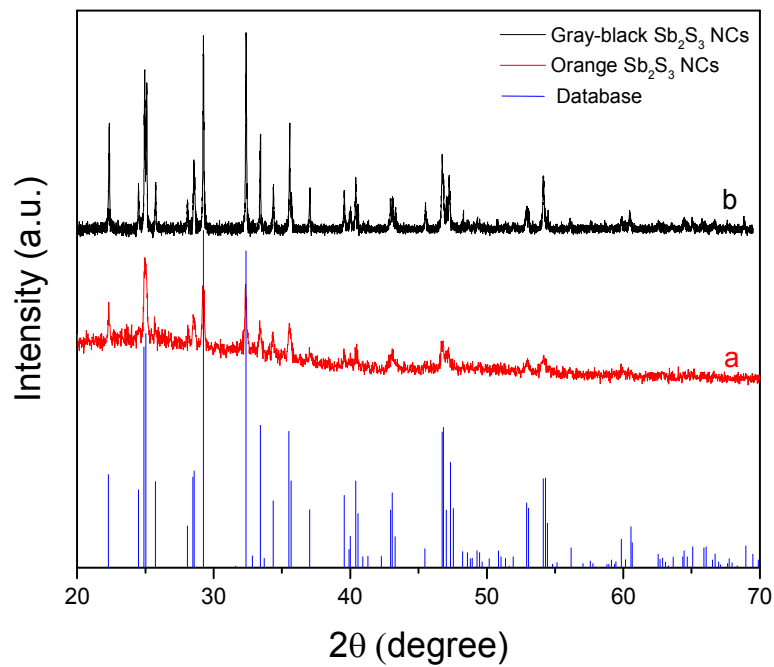
Figure 1. XRD patters of the as-synthesized Sb₂S₃ NCs.
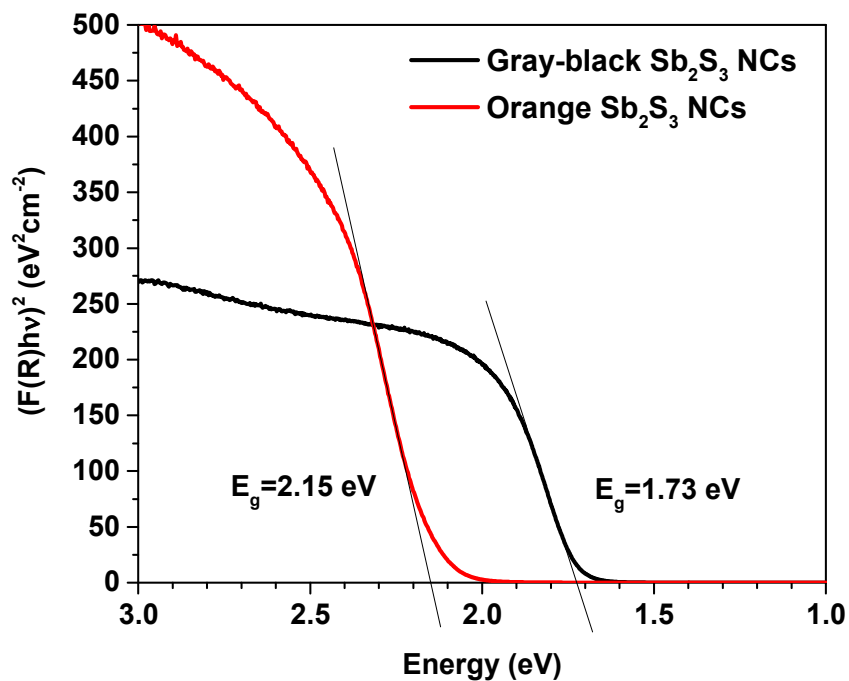
Figure 2. Tauc plots of as-synthesized orange and gray-black Sb_2S_3 NCs film on glass substrate. From the onsets of the plots the band gaps were estimated to be 2.15 eV for the orange and 1.73 eV for the gray-black Sb_2S_3 NCs.
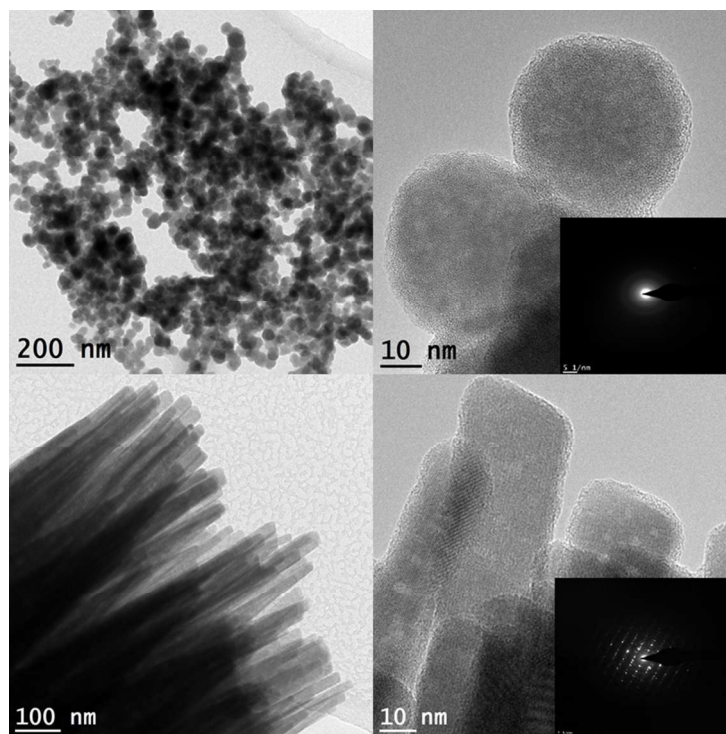
Figure 3. Electron micrographs of as –synthesized Sb$_2$S$_3$ NCs using Sb$_2$Cl$_3$, where the TMS solution was injected at 180 °C.(a) TEM, and (b) HRTEM images of Sb$_2$S$_3$ NCs after 90s since injection.
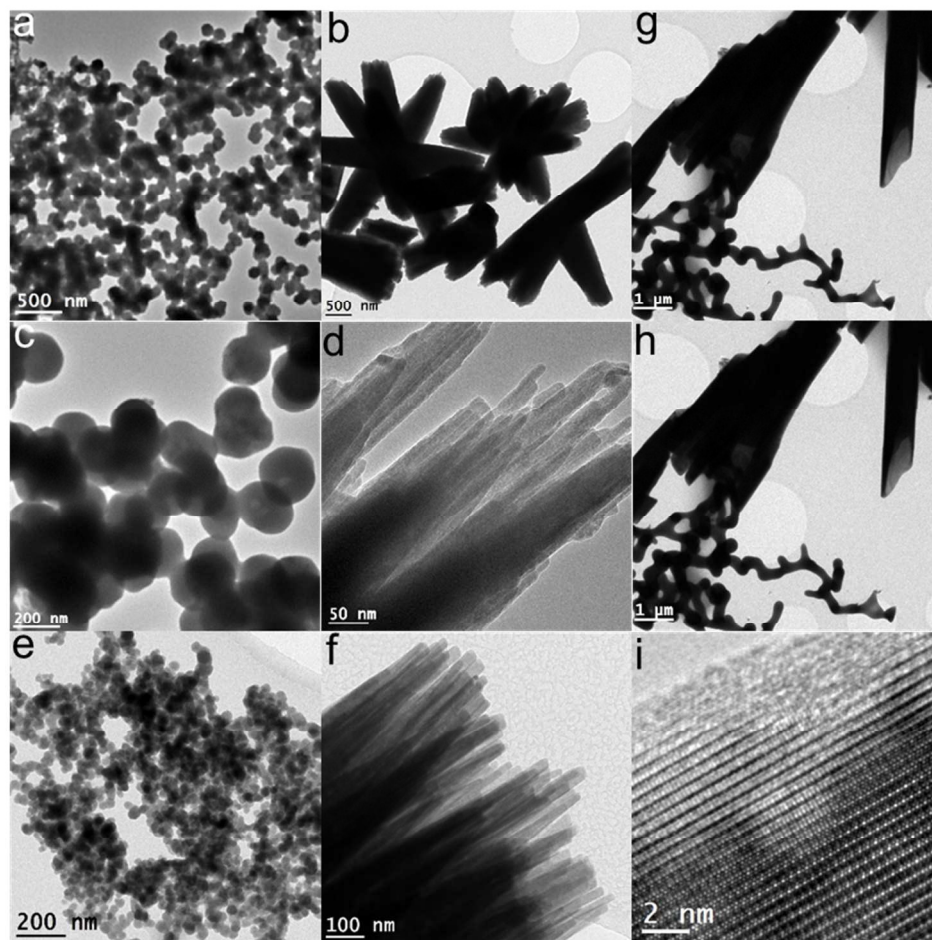
Figure 4. TEM and HRTEM electron micrographs of Sb$_2$S$_3$ NCs with TMS solution injected at different temperatures and left for different reaction times. After the injection, the temperature of all was reduced to 100°C. a) 100°C, 90 s; b) 100°C, 3 h; c) 140°C, 90 s; d) 140°C, 2 h; e) 180°C, 90 s; f) 180°C, 90 min; g) 230°C, 90 s; h) and i) 230°C, 90 min.
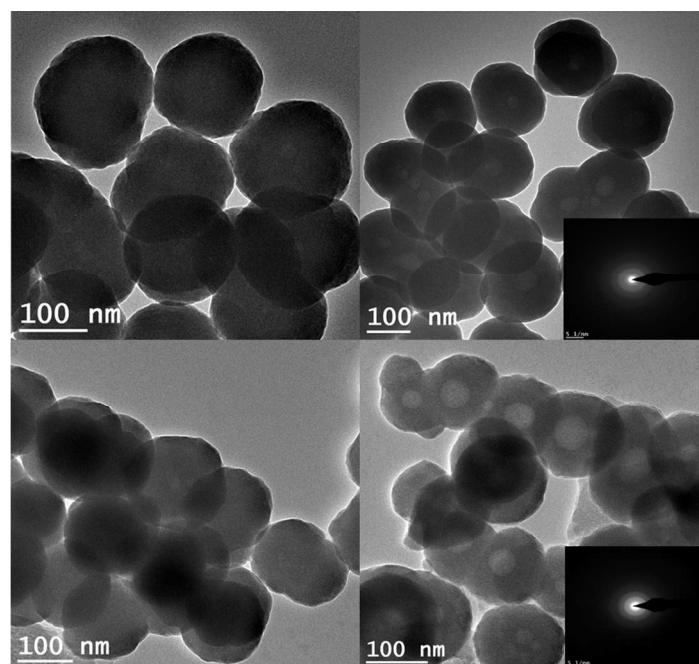
Figure 5. TEM and SAED electron micrographs of Sb$_2$S$_3$ NCs synthesized with different reaction times a) 90 s and b) 90 minutes using Sb(OAc)$_3$ precursor. C) 90s, an d) 90 minutes using Sb$_2$O$_3$ precursor.
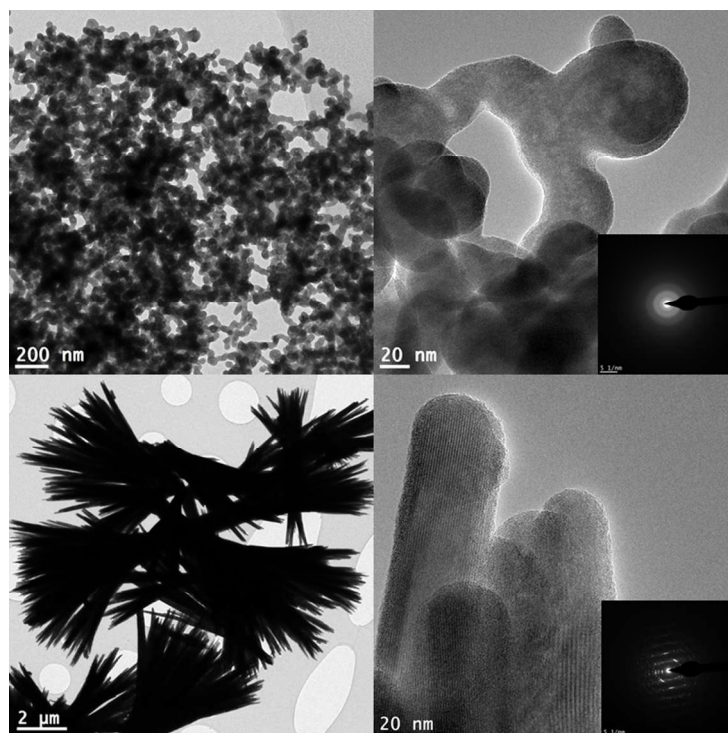
Figure 6. TEM, HRTEM and SAED micrographs of Sb$_2$S$_3$ NCs synthesized in the presence of chlorine source.

14
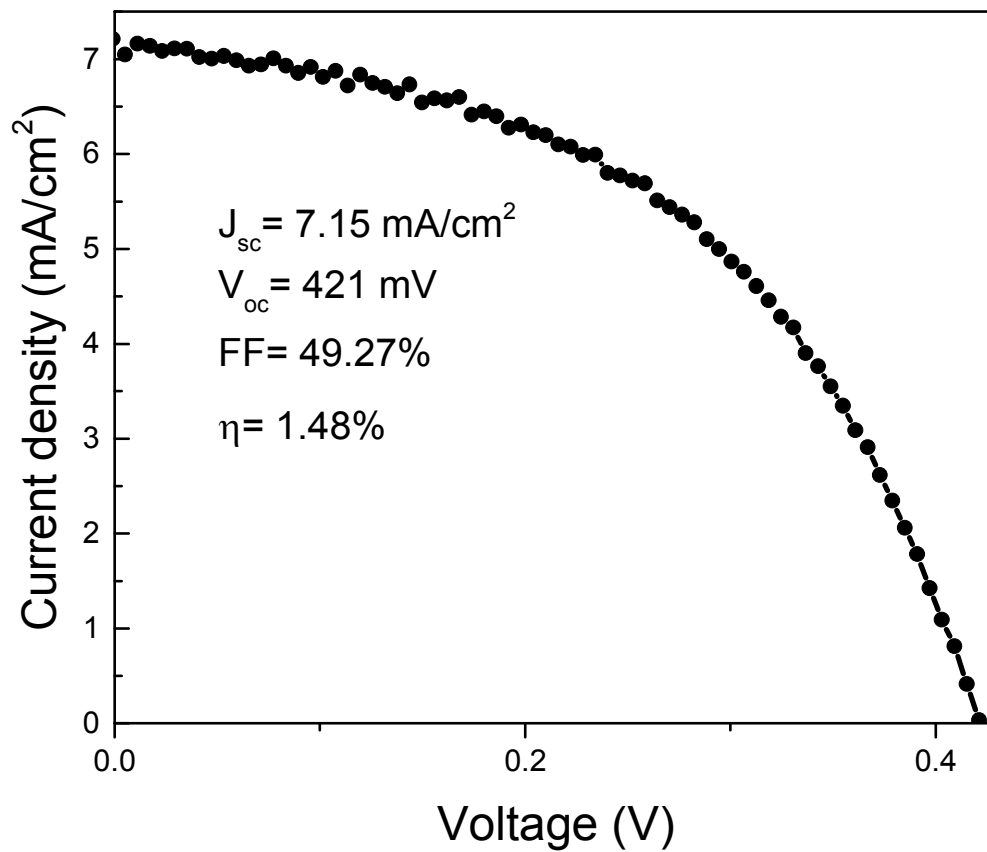
Figure 7 .The J-V curve of FTO/d-TiO$_2$/meso-TiO$_2$/Sb$_2$S$_3$/Spiro-OMeTAD/Au

Table of content (TOC)

Antimony sulfide nanocrystals with various-shape and different phases are synthesized using colloidal hot-injection method, and the as-prepared nanocrystals are used as light harvesting material in photovoltaic devices.
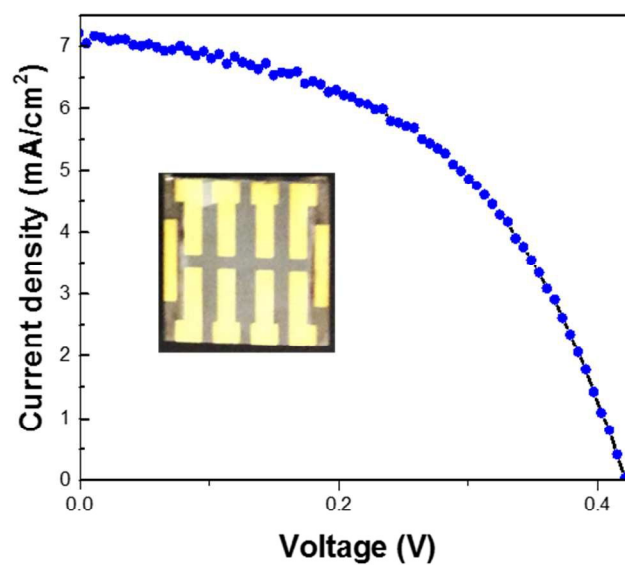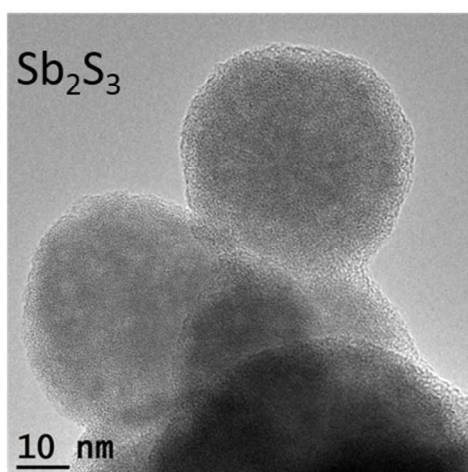
References:

1. M. Kuno, J. K. Lee, B. O. Dabbousi, F. V. Mikulec and M. G. Bawendi, *The Journal of Chemical Physics*, 1997, **106**, 9869-9882.
2. R. L. Z. Hoye, B. Ehrler, M. L. Böhm, D. Muñoz-Rojas, R. M. Altamimi, A. Y. Alyamani, Y. Vaynzof, A. Sadhanala, G. Ercolano, N. C. Greenham, R. H. Friend, J. L. MacManus-Driscoll and K. P. Musselman, *Advanced Energy Materials*, 2014, **4**, n/a-n/a.
3. Y. C. Choi, D. U. Lee, J. H. Noh, E. K. Kim and S. I. Seok, *Advanced Functional Materials*, 2014, **24**, 3587-3592.
4. Y. Zhou, M. Leng, Z. Xia, J. Zhong, H. Song, X. Liu, B. Yang, J. Zhang, J. Chen, K. Zhou, J. Han, Y. Cheng and J. Tang, *Advanced Energy Materials*, 2014, **4**, n/a-n/a.
5. Y. Du, Z. Yin, J. Zhu, X. Huang, X.-J. Wu, Z. Zeng, Q. Yan and H. Zhang, *Nat Commun*, 2012, **3**, 1177.
6. M. A. Becker, J. G. Radich, B. A. Bunker and P. V. Kamat, *The Journal of Physical Chemistry Letters*, 2014, **5**, 1575-1582.
7. M. G. Panthani, J. M. Kurley, R. W. Crisp, T. C. Dietz, T. Ezzyat, J. M. Luther and D. V. Talapin, *Nano Letters*, 2013, **14**, 670-675.
8. X. Liu, C. Chen, L. Wang, J. Zhong, M. Luo, J. Chen, D.-J. Xue, D. Li, Y. Zhou and J. Tang, *Progress in Photovoltaics: Research and Applications*, 2015, **23**, 1828-1836.
9. Y. Zhou, L. Wang, S. Chen, S. Qin, X. Liu, J. Chen, D.-J. Xue, M. Luo, Y. Cao, Y. Cheng, E. H. Sargent and J. Tang, *Nat Photon*, 2015, **9**, 409-415.
10. P. P. Boix, Y. H. Lee, F. Fabregat-Santiago, S. H. Im, I. Mora-Sero, J. Bisquert and S. I. Seok, *ACS Nano*, 2011, **6**, 873-880.
11. J. A. Chang, J. H. Rhee, S. H. Im, Y. H. Lee, H.-j. Kim, S. I. Seok, M. K. Nazeeruddin and M. Gratzel, *Nano Letters*, 2010, **10**, 2609-2612.
12. J. A. Chang, S. H. Im, Y. H. Lee, H.-j. Kim, C.-S. Lim, J. H. Heo and S. I. Seok, *Nano Letters*, 2012, **12**, 1863-1867.
13. C.-S. Lim, S. H. Im, J. H. Rhee, Y. H. Lee, H.-J. Kim, N. Maiti, Y. Kang, J. A. Chang, M. K. Nazeeruddin, M. Gratzel and S. I. Seok, *Journal of Materials Chemistry*, 2012, **22**, 1107-1111.
14. J. A. Christians and P. V. Kamat, *ACS Nano*, 2013, **7**, 7967-7974.
15. H. Wedemeyer, J. Michels, R. Chmielowski, S. Bourdais, T. Muto, M. Sugiura, G. Dennler and J. Bachmann, *Energy & Environmental Science*, 2013, **6**, 67-71.
16. S.-J. Moon, Y. Itzhaik, J.-H. Yum, S. M. Zakeeruddin, G. Hodes and M. Grätzel, *The Journal of Physical Chemistry Letters*, 2010, **1**, 1524-1527.
17. N. Bansal, F. T. F. O'Mahony, T. Lutz and S. A. Haque, *Advanced Energy Materials*, 2013, **3**, 986-990.
18. S. Messina, M. T. S. Nair and P. K. Nair, *Thin Solid Films*, 2009, **517**, 2503-2507.
19. A. M. S. a. M. S. Selim, *J. Phys. D: Appl. Phys.*, 2011, **34**.
20. F. Perales, G. Lifante, F. Agulló-Rueda and C. d. l. Heras, *Journal of Physics D: Applied Physics*, 2007, **40**, 2440.
21. S. Shaji, A. Arato, J. J. O'Brien, J. Liu, G. A. Castillo, M. I. M. Palma, T. K. D. Roy and B. Krishnan, *Journal of Physics D: Applied Physics*, 2010, **43**, 075404.
22. H. Bao, X. Cui, C. M. Li, Q. Song, Z. Lu and J. Guo, *The Journal of Physical Chemistry C*, 2007, **111**, 17131-17135.
23. C.-M. Park, Y. Hwa, N.-E. Sung and H.-J. Sohn, *Journal of Materials Chemistry*, 2010, **20**, 1097-1102.
24. B. N. Reddy, M. Deepa and A. G. Joshi, *Physical Chemistry Chemical Physics*, 2014, **16**, 2062-2071.
25. M. Y. Versavel and J. A. Haber, *Thin Solid Films*, 2007, **515**, 7171-7176.

26.   O. S. andK.C.Mandal, *J. Electrochem. Soc.*, 1992, **139**.
27.   A. Alemi, S. W. Joo, Y. Hanifehpour, A. Khandar, A. Morsali and B.-K. Min, *Journal of Nanomaterials*, 2011, **2011**, 5.
28.   H. Hu, Z. Liu, B. Yang, M. Mo, Q. Li, W. Yu and Y. Qian, *Journal of Crystal Growth*, 2004, **262**, 375-382.
29.   X. Chen, X. Zhang, C. Shi, X. Li and Y. Qian, *Solid State Communications*, 2005, **134**, 613-615.
30.   J. Yang, J.-h. Zeng, S.-H. Yu, L. Yang, Y.-H. Zhang and Y.-T. Qian, *Chemistry of Materials*, 2000, **12**, 2924-2929.
31.   R. Zhang, X. Chen, M. Mo, Z. Wang, M. Zhang, X. Liu and Y. Qian, *Journal of Crystal Growth*, 2004, **262**, 449-455.
32.   J. Rodriguez-Castro, M. F. Mahon and K. C. Molloy, *Chemical Vapor Deposition*, 2006, **12**, 601-607.
33.   J. R. Castro, P. Dale, M. F. Mahon, K. C. Molloy and L. M. Peter, *Chemistry of Materials*, 2007, **19**, 3219-3226.
34.   J. R. Castro, K. C. Molloy, Y. Liu, C. S. Lai, Z. Dong, T. J. White and E. R. T. Tiekink, *Journal of Materials Chemistry*, 2008, **18**, 5399-5405.
35.   H. Li, D. Chen, L. Li, F. Tang, L. Zhang and J. Ren, *CrystEngComm*, 2010, **12**, 1127-1133.
36.   Y. Guo, S. R. Alvarado, J. D. Barclay and J. Vela, *ACS Nano*, 2013, **7**, 3616-3626.
37.   V. I. Klimov, *Semiconductor and Metal Nanocrystals*, Marcel Dekker, Inc., 2004.
38.   N. Maiti, S. H. Im, Y. H. Lee and S. I. Seok, *ACS Applied Materials & Interfaces*, 2012, **4**, 4787-4791.
39.   M. R. Langille, M. L. Personick, J. Zhang and C. A. Mirkin, *Journal of the American Chemical Society*, 2012, **134**, 14542-14554.
40.   Z. Zhao, Z. Zhou, J. Bao, Z. Wang, J. Hu, X. Chi, K. Ni, R. Wang, X. Chen, Z. Chen and J. Gao, *Nat Commun*, 2013, **4**.
41.   W. Li, R. Zamani, M. Ibáñez, D. Cadavid, A. Shavel, J. R. Morante, J. Arbiol and A. Cabot, *Journal of the American Chemical Society*, 2013, **135**, 4664-4667.
42.   Y. C. Choi, T. N. Mandal, W. S. Yang, Y. H. Lee, S. H. Im, J. H. Noh and S. I. Seok, *Angewandte Chemie*, 2014, **126**, 1353-1357.